Research Square

Preprints are preliminary reports that have not undergone peer review.
They should not be considered conclusive, used to inform clinical practice,
or referenced by the media as validated information.

ROI-free and Automated Detection of the Cervical Ossification of the Posterior Longitudinal Ligament on MRI Based on Deep Learning

Yida Wang
Affiliated Hospital of Qingdao University
Weihang Zhu
Affiliated Hospital of Qingdao University
Lu Zhang
Affiliated Hospital of Qingdao University
Zihan Cui
Qingdao University
Hengsen Xu
Affiliated Hospital of Qingdao University
Ning Yu
Affiliated Hospital of Qingdao University
Hao Zhang
Affiliated Hospital of Qingdao University
Chao Wang
dr_wangchao@hotmail.com
Affiliated Hospital of Qingdao University

Research Article

Keywords: Ossification, Posterior longitudinal ligament, Artificial intelligence, Deep learning

Posted Date: November 23rd, 2026

DOI: https://doi.org/10.21203/rs.3.rs-11189594/v1

License: This work is licensed under a Creative Commons Attribution 4.0 International License.
Read Full License

Additional Declarations: No competing interests reported.

ROI-free and Automated Detection of the Cervical Ossification of the Posterior Longitudinal Ligament on MRI Based on Deep Learning

Abstract

Background and Objectives: To develop a region of interest (ROI)-free model for ossification of the posterior longitudinal ligament (OPLL) identification and diagnosis in cervical MRI with interpretable feature representations.

Methods: A total of 4861 cervical MRI images of 1028 patients from 3 hospitals were enrolled and divided into the training, validation, and external test datasets. We evaluated the performance of the ROI-free and automated cervical OPLL (RACO) model based on the area under the receiver operating characteristic (ROC) curves, feature attention maps, accuracy, sensitivity, and specificity. In addition, we also evaluated the effectiveness of the RACO model in the different OPLL types.

Results: The AUC of the RACO model was 0.91 and 0.88 in the validation and external test datasets, respectively. In the validation dataset, the AUCs of ResNet-101, EfficientNet-S, and Shufflenet models were 0.52, 0.53 and 0.62, respectively. Grad-CAM showed that the RACO model generated accurate peak responses on the target area. In addition, the RACO model showed the highest accuracy in the continuous subgroup (97.08%) and the lowest accuracy in the localized subgroup (93.82%).

Conclusion: The RACO model showed excellent performance, and interpretable attention maps may support clinical decision-making and reduce radiation exposure for patients.

Keywords: Ossification; Posterior longitudinal ligament; Artificial intelligence; Deep learning

Key Points:

We developed and externally validated a deep learning model for OPLL detection on cervical MRI in a multicentre cohort of 1028 patients (4861 images), the largest reported to date.

The model takes whole sagittal MRI slices as input and requires no manual ROI segmentation, which removes the main bottleneck for clinical deployment.

The model can provide interpretable attention maps to support the prediction results.

Abbreviations:

OPLL: ossification of the posterior longitudinal ligament; ROI: region of interest; RACO: ROI-free and automated cervical OPLL; ROC: receiver operating characteristic; AUC: area under the receiver operating characteristic curve; MRI: magnetic resonance imaging; CT: computed tomography; DL:

deep learning; Grad-CAM: gradient-weighted class activation mapping; ML: machine learning; SHAP: Shapley additive explanation.

Introduction

Ossification of the posterior longitudinal ligament (OPLL) is characterized by the pathological osteogenic transition and hyperplasia of the posterior longitudinal ligament, predominantly at the cervical and thoracic spine[1]. OPLL can result in the formation of osseous spurs that impinge on the spinal cord and nerves, which is one of the most important causes of cervical spinal canal stenosis and compression of the spinal cord in East Asians[2-4]. The prevalence of this disease is 1.9% to 4.3% in Japan[5]. Neurological deficits may arise along with the progression of the ossification, which finally necessitates the surgical resection of the lesion and thus decompression of the neural structures[2]. The symptoms usually progress over time, so early detection of OPLL is critical for both the prevention and intervention of the irreversible disease[6].

Magnetic resonance imaging (MRI) has been regarded as the most reliable imaging technique for evaluating the compression of the spinal cord. MRI is a highly preferred diagnostic tool in outpatient settings because it can accurately identify soft tissues without ionizing radiation exposure. However, on MRI, ossified lesions appear as low-signal areas on all sequences and are difficult to distinguish from the adjacent posterior longitudinal ligament, dura, and cerebrospinal fluid; consequently, even experienced spine surgeons and radiologists may miss or misclassify OPLL[7]. Computed tomography (CT) is frequently utilized in clinical practice and regarded as the gold standard for diagnosing OPLL[8]. CT is always required in patients who are highly suspected of OPLL, even if they have undergone MRI. In other words, for patients with a high suspicion of OPLL, a combination of MRI and CT scans is frequently required to compensate for the limitations of each test. However, this combined approach increases cost and radiation exposure and reduces patients' willingness to undergo repeated examinations. As a result, diagnosis is often delayed and the yield of opportunistic screening for OPLL remains low.

Deep learning (DL), one of the significant technologies in the field of artificial intelligence, has emerged as the leading method in machine learning[9]. Deep learning uses multilayer neural networks to learn hierarchical feature representations directly from raw data, without hand-crafted feature engineering[10]. Neural networks, particularly those with many hidden layers, are the foundation of deep learning, which is also where the term "deep" comes from. With the advancement of DL in artificial intelligence and radiomics in recent years, numerous models have demonstrated efficacy in supporting clinical decision-making[7, 11, 12]. For instance, Zhang et al. used clinical and ultrasound-based radiomics to build an optimal model to predict the response of patients with axillary lymph node-positive breast cancer to neoadjuvant chemotherapy[11]. However, to the best of our knowledge, few studies have concentrated on DL models for the identification and detection of OPLL from cervical MRI.

In this study, we aim to develop a region of interest (ROI)-free model for OPLL identification and diagnosis in cervical MRI with interpretable feature representations. Furthermore, we compared it to other DL models, and externally validated and tested the model and explored whether it remains highly accurate for an external test dataset.

Methods

Study design and patients

The overall study design, image pre-processing pipeline, and model evaluation framework have been described in detail in our previous multicentre study on spinal imaging[13]. The present work applies the same framework to cervical MRI for OPLL detection; only OPLL-specific procedures and any deviations from that protocol are described below. In this multi-institutional retrospective study, 4972 participants who underwent both cervical CT and MRI for all clinical indications at Hospitals A, B, and C from July 2016 to September 2022 were initially included. This study was approved by the Ethics Committee of Affiliated Hospital of Qingdao University and was conducted in accordance with the ethical principles of the Declaration of Helsinki. We

used pre-existing medical data only; therefore, the requirement for informed consent was waived for this retrospective study.

According to the exclusion criteria, we excluded 3944 patients, including those for whom more than 3 months elapsed between CT and MRI (n=2149); those who had previously undergone cervical spine surgery, including laminectomy with instrumented fusion and single- or double-door open-door laminoplasty (n=957) and those who lacked complete raw data or qualified CT/MRI images (n=838).

Finally, 4861 cervical MRI images of 1028 patients were enrolled, and the patients from Hospital A were divided into the training dataset (3760 images of 689 patients). To assess the external generalizability of our DL models, the patients from Hospital B were divided into the validation dataset (570 images of 169 patients) and the patients from Hospital C were divided into the external test dataset (531 images of 170 patients). The study flowchart is displayed in Fig. 1.

Diagnosis of cervical OPLL

Reference labels were assigned on the basis of cervical 3D CT, with no ROI segmented or delineated at any stage. OPLL was classified according to the Tsuyama criteria[5, 14] as continuous, segmental, mixed, or localised type on the basis of the morphology of the ossified mass. Sagittal MRI and CT images were reviewed by one radiologist and one spine surgeon, and any disagreement was resolved by consensus discussion.

Radiological examination

The primary MRI equipment used by patients from Hospital A was a Siemens Skyra 3.0-T MRI (Siemens AG) equipped with a spine array coil. Patients from Hospital B primarily used a Philips Achieva 1.5-T MRI, while patients from Hospital C primarily used a Philips Achieva 1.5-T MRI equipped with a spine array coil.

Model development

As noted above, model development followed the framework used in our previous study[13]. Briefly, the classifier was based on a 34-layer residual network (ResNet-34)

initialised with ImageNet weights and fine-tuned on the training set. Images were resized and augmented as previously described[13]. Training used the Adam optimiser with a learning rate of 0.0001 for 200 epochs, and all models were implemented in PyTorch.

Model test and evaluation

External-test performance was assessed using the frozen training weights and the same operating threshold applied throughout. Three widely used architectures, ResNet-101[15], Shufflenet[16], and Efficientnet-S[17] were trained and evaluated as benchmarks under identical conditions. Discrimination was described by the area under the receiver operating characteristic curve (AUC), together with sensitivity, specificity, and accuracy.

Visualization

To identify which image regions drove each prediction, class activation maps were generated for all models using Grad-CAM[18, 19]. following the implementation described in our previous study[13].

Subgroup analysis

We additionally examined whether diagnostic performance differed across the four OPLL morphologies, which vary considerably in lesion size. Patients in the validation and external test sets were grouped by the CT-based morphological subtype (continuous, segmental, mixed, or localised), and performance was compared between groups..

Statistical analysis

Continuous variables are summarised as mean±SD and categorical variables as counts (%). Between-group comparisons used the Student's t-test or the Mann–Whitney U test for continuous variables, as appropriate, and the χ^2 or Fisher's exact test for categorical variables. Statistical significance was defined as two-sided $P < 0.05$. Analyses were carried out in SPSS Statistics (version 22.0) and Python (version 3.7).

Results

Population characteristics

A total of 689 patients were enrolled in the training dataset, 223 patients (70 male and 153 female; mean age: 61.13±10.22 years) were diagnosed with OPLL, comprising 25 (11.21%) continuous, 106 (47.53%) segmental, 31 (13.90%) mixed, and 61 (27.35%) localized. In addition, 466 patients (173 male and 293 female; mean age: 59.02±11.01 years) were in the non-OPLL group. The validation dataset from Hospital B included 169 patients in total, 62 patients (38 male and 24 female; mean age: 61.35±9.21 years) were diagnosed with OPLL, included 2 (3.23%) continuous, 34 (54.84%) segmental, 6 (9.68%) mixed, and 20 (32.26%) localized. The external test dataset included 170 patients in total, 84 patients (57 male and 27 female; mean age: 60.19±10.54 years) were diagnosed with OPLL, comprising 12 (14.29%) continuous, 26 (30.95%) segmental, 8 (9.52%) mixed, and 38 (45.24%) localized. Detailed demographics of each cohort were shown in Table 1.

Performance of models

The AUC of the RACO model was 0.91 and 0.88 in the validation and external test datasets, respectively. In the validation dataset, the AUCs of ResNet-101, Efficientnet-S, and Shufflenet models were 0.52, 0.53 and 0.62, respectively. In the external test dataset, the AUCs of ResNet-101, Efficientnet-S, and Shufflenet models were 0.48, 0.51 and 0.47, respectively (Fig. 2).

In addition, in the validation dataset, the accuracy, sensitivity, and specificity of the RACO model were 93.16%, 81.94% and 96.95%, respectively; in external test dataset, the accuracy, sensitivity, and specificity of the RACO model are 91.71%, 79.64% and 97.25%, respectively. The accuracy, sensitivity, and specificity of the other models are listed in Table 2.

Visualization

Grad-CAM showed that the RACO model generated accurate peak responses on the target area for images that were correctly classified, the prediction of OPLL was primarily done with accurate focus on the dorsal part of the vertebral body. In addition, ResNet-101, Efficientnet-S, and Shufflenet models generated low-intensity or absent activation, or activation outside the target region (Fig. 3 and 4).

Subgroup analysis

In the four subgroups (continuous, segmental, mixed, and localized), the AUCs of the RACO model were 0.97, 0.91, 0.94 and 0.82, respectively (Fig. 5). In addition, the RACO model showed the highest accuracy in the continuous subgroup (97.08%) and the lowest accuracy in localized subgroup (93.82%). The accuracy, sensitivity, and specificity of the RACO model for the other subgroups are listed in Table 3.

Discussion

OPLL belongs to a group of systematic ossification of the spinal ligaments and has high prevalence in Eastern Asia, particularly in China, Japan, and South Korea[20]. When considering the surgical approaches and associated risks, it is important for clinicians to differentiate OPLL from other cervical compressive myelopathies. The selection of a surgical approach for patients with cervical OPLL necessitates the utmost caution. In cases where the bone mass is substantial or situated posteriorly to the vertebral body, the conventional discectomy procedure may encounter challenges in accessing the lesion site. This not only raises the possibility of a surgical failure but also increases the risk of potential damage to the dura mater and nerves[4, 7]. Consequently, CT is necessary for each patient to demonstrate and assess the OPLL. Nevertheless, it is impossible to overlook the drawbacks of CT scans, such as their high radiation exposure. Deep learning and radiomics models have shown efficacy in supporting clinical decision-making across imaging tasks[21-24]. In the present study we developed and externally validated the RACO model for OPLL detection on cervical MRI. The model reached an AUC of 0.91 in the validation set and 0.88 in the external test set without

any manual ROI delineation, and its activation maps corresponded to the ossified region seen on CT (Figures 3, 4).

ROI-Free and Visualization

With the advancement of radiomics and artificial intelligence, DL and machine learning (ML) models have been investigated for the diagnosis and prognosis of numerous diseases[25]. Most published radiomics and deep-learning pipelines for spinal disorders rely on manually delineated lesion ROIs, an approach that is labour-intensive and is widely recognised as a barrier to clinical deployment[11, 12, 26]. As a result, we developed the RACO model which enhances the model flexibility, reduces the complexity of segmentation, and eliminates the need for a predefined lesion ROI. In addition, our RACO model may be able to extract more features from OPLL peri-structures, such as spinal cord compression and intramedullary signal intensity, than the ROI of lesion. In fact, many studies have paid more attention to evaluate the significance of intramedullary signal intensity in OPLL and ossification of the ligamentum flavum[27].

Many studies have demonstrated that traditional classification models can achieve encouraging results without ROI requirement, nevertheless, the lack of interpretability in these models prevents their widespread implementation. Interpretability is a crucial factor that most physicians consider when using DL models to support their decision-making[28]. However, it is challenging to overcome the “black-box” issue and get the correct and intuitive interpretation of DL and ML models. Hu et al. developed an ML model for early prediction of acute kidney injury in critically ill children, and provide the explanations for the model via the SHAP method[29, 30]. Compared with the three benchmark architectures, the RACO model produced more focal activation that localised to the posterior vertebral margin, whereas the benchmarks showed diffuse or off-target activation (Figures 3 and 4).

Model Performance

More trained images included in the dataset may often represent higher model

performance. And the models that are developed based on dataset that include fewer positive patients may be prone to overfitting. In the present study, 223 OPLL patients were collected to develop and enhance the robustness of our RACO model. Shemesh et al. developed a novel DL model to identify cervical OPLL on MRI without the use of CT scans, however, the images used for development and testing were obtained from a single tertiary referral hospital[7]. In other words, the external generalizability of the model was not evaluated in the above study. In the present study, validation and external test datasets were used to assess the external generalizability of the RACO model, and high AUC was achieved.

In addition, all OPLL subtypes were included in this study to evaluate whether the performance of the RACO model would be affected by the morphology of the OPLL. Performance was lowest in the localised subtype (AUC 0.82), which we attribute to the small size of the ossified mass in these cases. Because all four subtypes exceeded an AUC of 0.80, however, overall diagnostic performance did not appear to depend materially on OPLL morphology.

Limitations

There are some limitations to this study. Although our study included a larger number of OPLL patients than previous studies, larger samples and more centres are still required. Especially, more external independent verification datasets are required to verify the ability of our models in clinical applications. Additionally, in the present study, only sagittal MRI images were used to identify OPLL, and the lack of 3D MRI may have resulted in the loss of some features and decreased the sensitivity of our model. Finally, while 3D CT is the diagnostic gold standard for OPLL, biases and inherent differences in classification results were inevitable in the present retrospective study.

Conclusions

In the present study, we developed the RACO model for ROI-free and automated

diagnosis of OPLL from spinal MRI. The excellent performance and interpretable attention maps may support early clinical decision-making and reduce radiation exposure for patients suffering the disease.

Authors

Yida Wang[1†], Weihang Zhu[1†], Lu Zhang[2], Zihan Cui[3], Hengsen Xu[1], Ning Yu[1], Hao Zhang[1*], Chao Wang[1*]

[1]Department of Spine Surgery, the Affiliated Hospital of Qingdao University, Qingdao, Shandong, China

[2]Department of Medical Research Center, the Affiliated Hospital of Qingdao University, Qingdao, Shandong, China

[3]Qingdao Medical College, Qingdao University, Qingdao, China

* Corresponding author:

Chao Wang, M.D.

Department of Spine Surgery

the Affiliated Hospital of Qingdao University

No.59 Haier Road, Qingdao, Shandong, China 266000.

Email: dr_wangchao@hotmail.com.

Hao Zhang, M.D.

Department of Spine Surgery

the Affiliated Hospital of Qingdao University

No.59 Haier Road, Qingdao, Shandong, China 266000.

E-mail: zhanghaospinal1995@163.com

Consent to participate declaration

Not applicable. This was a retrospective study using pre-existing medical data. The requirement for informed consent was waived by the Ethics Committee of Affiliated

Hospital of Qingdao University.

Ethics Approval declaration

This study was approved by the Ethics Committee of Affiliated Hospital of Qingdao University (approved No. of ethic committee: QYFYWZLL28007). This study also was conducted in accordance with the ethical principles of the Declaration of Helsinki.

Consent for publication

Not applicable.

Availability of data and materials

The datasets used and/or analysed during the current study are available from the corresponding author on reasonable request.

Funding

This work was supported by the National Natural Science Foundation of China (No. 82071667, 81902209).

References

1. Boody BS, Lendner M, Vaccaro AR: **Ossification of the posterior longitudinal ligament in the cervical spine: a review**. *Int Orthop* 2019, **43**(4):797-805.
2. Zhang Q, Guo R, Fang S, Tong S, Fan Y, Wang J: **The clinical efficacy of laminectomy fusion fixation and posterior single open-door laminoplasty in the treatment of multilevel cervical ossification of the posterior longitudinal ligament (OPLL): a retrospective study**. *BMC Surg* 2023, **23**(1):380.
3. Lee SY, Shin YR, Park HJ, Rho MH, Chung EC: **Usefulness of multiecho fast field echo MRI in the evaluation of ossification of the posterior longitudinal ligament and dural ossification of the cervical spine**. *PLoS One* 2017, **12**(8):e0183744.
4. Wu JC, Chen YC, Huang WC: **Ossification of the Posterior Longitudinal Ligament in Cervical Spine: Prevalence, Management, and Prognosis**. *Neurospine* 2018, **15**(1):33-41.
5. Le HV, Wick JB, Van BW, Klineberg EO: **Ossification of the Posterior Longitudinal**

Ligament: Pathophysiology, Diagnosis, and Management. *J Am Acad Orthop Surg* 2022, **30**(17):820-830.

6. Li H, Dai LY: **A systematic review of complications in cervical spine surgery for ossification of the posterior longitudinal ligament**. *Spine J* 2011, **11**(11):1049-1057.
7. Shemesh S, Kimchi G, Yaniv G, Harel R: **MRI-based detection of cervical ossification of the posterior longitudinal ligament using a novel automated machine learning diagnostic tool**. *Neurosurg Focus* 2023, **54**(6):E11.
8. Chang H, Kong CG, Won HY, Kim JH, Park JB: **Inter- and intra-observer variability of a cervical OPLL classification using reconstructed CT images**. *Clin Orthop Surg* 2010, **2**(1):8-12.
9. McMaster C, Bird A, Liew DFL, Buchanan RR, Owen CE, Chapman WW, Pires DEV: **Artificial Intelligence and Deep Learning for Rheumatologists**. *Arthritis Rheumatol* 2022, **74**(12):1893-1905.
10. Schmidt-Erfurth U, Sadeghipour A, Gerendas BS, Waldstein SM, Bogunović H: **Artificial intelligence in retina**. *Prog Retin Eye Res* 2018, **67**:1-29.
11. Zhang H, Cao W, Liu L, Meng Z, Sun N, Meng Y, Fei J: **Noninvasive prediction of node-positive breast cancer response to presurgical neoadjuvant chemotherapy therapy based on machine learning of axillary lymph node ultrasound**. *J Transl Med* 2023, **21**(1):337.
12. Zhang H, Yuan G, Wang C, Zhao H, Zhu K, Guo J, Chen M, Liu H, Yang G, Wang Y *et al*: **Differentiation of benign versus malignant indistinguishable vertebral compression fractures by different machine learning with MRI-based radiomic features**. *Eur Radiol* 2023, **33**(7):5069-5076.
13. Zhang H, Xu R, Guo X, Zhou D, Xu T, Zhong X, Kong M, Zhang Z, Wang Y, Ma X: **Deep learning-based automated high-accuracy location and identification of fresh vertebral compression fractures from spinal radiographs: a multicenter cohort study**. *Front Bioeng Biotechnol* 2024, **12**:1397003.
14. Tsuyama N: **Ossification of the posterior longitudinal ligament of the spine**. *Clin Orthop Relat Res* 1984(184):71-84.
15. He K, Zhang X, Ren S, Sun J: **Deep residual learning for image recognition**. In: *Conference on Computer Vision and Pattern Recognition (CVPR): 2016*; 2016.
16. Zhang X, Zhou X, Lin M, Sun J: **Shufflenet: An extremely efficient convolutional neural network for mobile devices**. In: *Proceedings of the IEEE conference on computer vision and pattern recognition: 2018*; 2018: 6848-6856.
17. Tan M, Le Q: **Efficientnet: Rethinking model scaling for convolutional neural networks**. In: *International conference on machine learning: 2019*: PMLR; 2019: 6105-6114.
18. Panwar H, Gupta PK, Siddiqui MK, Morales-Menendez R, Bhardwaj P, Singh V: **A deep learning and grad-CAM based color visualization approach for fast detection of COVID-19 cases using chest X-ray and CT-Scan images**. *Chaos Solitons Fractals* 2020, **140**:110190.
19. Liu C, Xie H, Zhang Y: **Self-Supervised Attention Mechanism for Pediatric Bone Age Assessment With Efficient Weak Annotation**. *IEEE Trans Med Imaging* 2021, **40**(10):2685-2697.
20. Hirabayashi S: **Ossification of the ligamentum flavum**. *Spine Surg Relat Res* 2017,

1(4):158-163.
21. Meng N, Wong KK, Zhao M, Cheung JPY, Zhang T: **Radiograph-comparable image synthesis for spine alignment analysis using deep learning with prospective clinical validation**. *EClinicalMedicine* 2023, **61**:102050.
22. Gitto S, Cuocolo R, Annovazzi A, Anelli V, Acquasanta M, Cincotta A, Albano D, Chianca V, Ferraresi V, Messina C *et al*: **CT radiomics-based machine learning classification of atypical cartilaginous tumours and appendicular chondrosarcomas**. *EBioMedicine* 2021, **68**:103407.
23. Liu X, Zhang D, Liu Z, Li Z, Xie P, Sun K, Wei W, Dai W, Tang Z, Ding Y *et al*: **Deep learning radiomics-based prediction of distant metastasis in patients with locally advanced rectal cancer after neoadjuvant chemoradiotherapy: A multicentre study**. *EBioMedicine* 2021, **69**:103442.
24. Huang Y, Zhu T, Zhang X, Li W, Zheng X, Cheng M, Ji F, Zhang L, Yang C, Wu Z *et al*: **Longitudinal MRI-based fusion novel model predicts pathological complete response in breast cancer treated with neoadjuvant chemotherapy: a multicenter, retrospective study**. *EClinicalMedicine* 2023, **58**:101899.
25. Jiang Y, Zhang Z, Yuan Q, Wang W, Wang H, Li T, Huang W, Xie J, Chen C, Sun Z *et al*: **Predicting peritoneal recurrence and disease-free survival from CT images in gastric cancer with multitask deep learning: a retrospective study**. *Lancet Digit Health* 2022, **4**(5):e340-e350.
26. Chen W, Liu X, Li K, Luo Y, Bai S, Wu J, Chen W, Dong M, Guo D: **A deep-learning model for identifying fresh vertebral compression fractures on digital radiography**. *Eur Radiol* 2022, **32**(3):1496-1505.
27. Zhang H, Wang C, Wang D, Zhou C, Zhu K, Tu Q, Kong M, Zhao C, Ma X: **Predictive Risk Factors of Poor Preliminary Postoperative Outcome for Thoracic Ossification of the Ligamentum Flavum**. *Orthop Surg* 2021, **13**(2):408-416.
28. Mo Y, Han C, Liu Y, Liu M, Shi Z, Lin J, Zhao B, Huang C, Qiu B, Cui Y *et al*: **HoVer-Trans: Anatomy-Aware HoVer-Transformer for ROI-Free Breast Cancer Diagnosis in Ultrasound Images**. *IEEE Trans Med Imaging* 2023, **42**(6):1696-1706.
29. Hu J, Xu J, Li M, Jiang Z, Mao J, Feng L, Miao K, Li H, Chen J, Bai Z *et al*: **Identification and validation of an explainable prediction model of acute kidney injury with prognostic implications in critically ill children: a prospective multicenter cohort study**. *EClinicalMedicine* 2024, **68**:102409.
30. Nohara Y, Matsumoto K, Soejima H, Nakashima N: **Explanation of machine learning models using shapley additive explanation and application for real data in hospital**. *Comput Methods Programs Biomed* 2022, **214**:106584.

Figures

Fig. 1. The study flowchart

Fig. 2. Performance of the models in the validation and external test datasets. ROC curves of models in (A) the validation dataset and (B) the external test dataset.

Fig. 3. Attention heatmaps of different models for representative non-OPLL patient.

Fig. 4. Attention heatmaps of different models for representative OPLL patient.

Fig. 5. Performance of the RACO model in the subgroups. ROC curves of the RACO model in (A) the mixed group, (B) the segmental group, (C) the localized group, and (D) the continuous group.

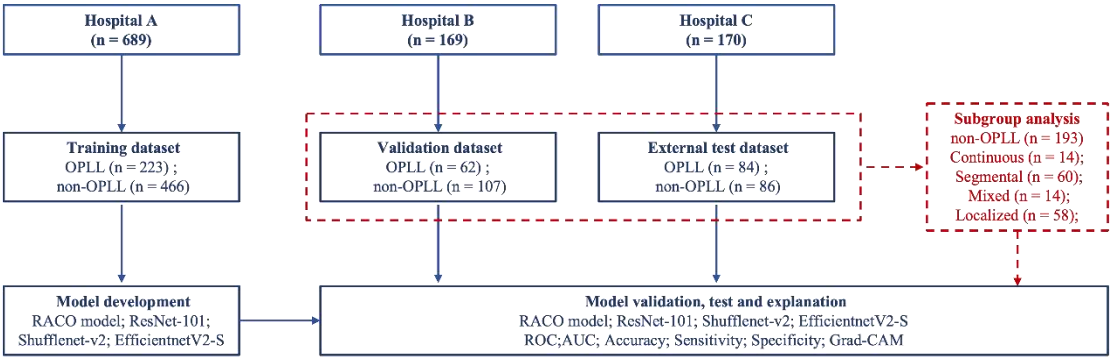

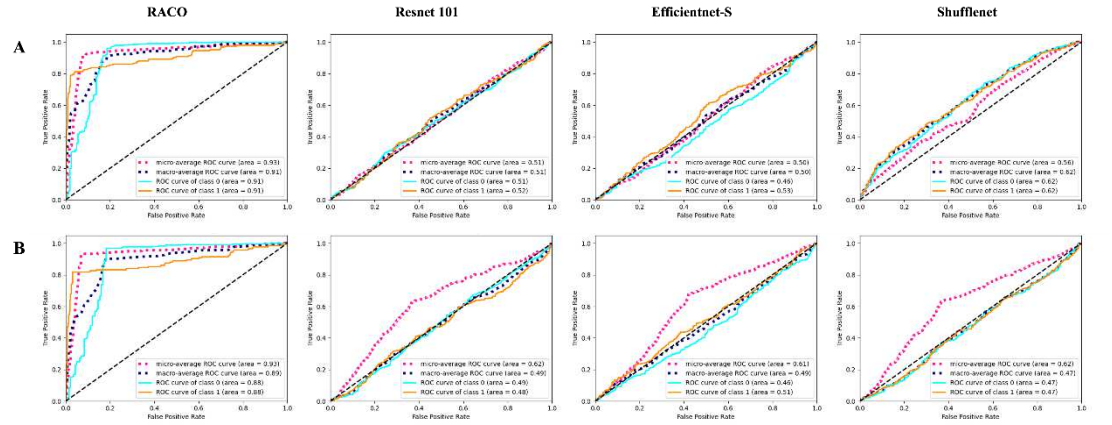

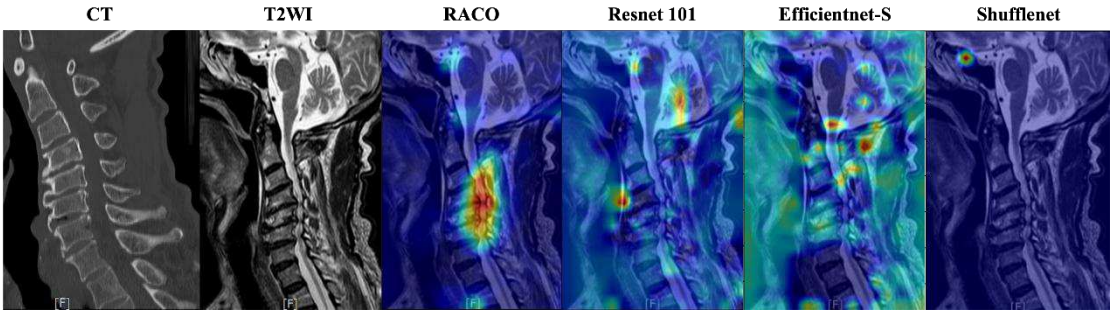

423

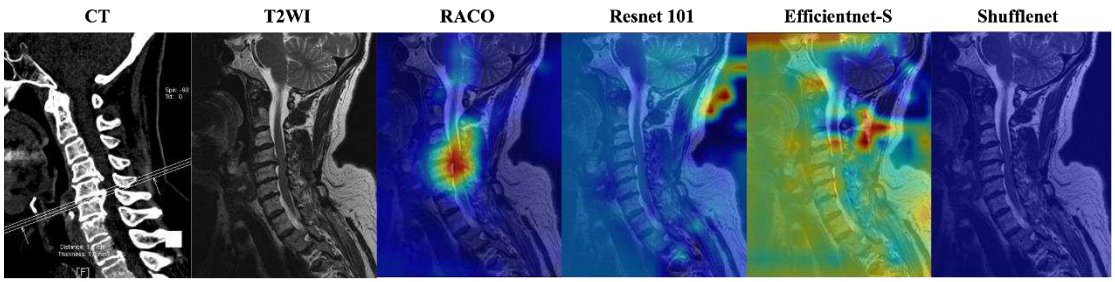
CT
T2WI
RACO
Resnet 101
Efficientnet-S
Shufflenet

424

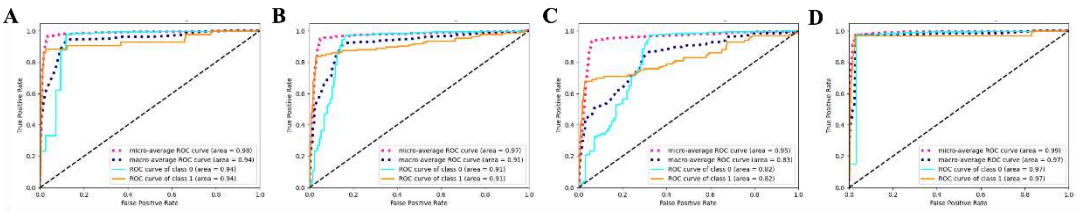
A
B
C
D
True Positive Rate
False Positive Rate

Supplementary Files

This is a list of supplementary files associated with this preprint. Click to download.

- Table2.docx
- Table1.docx
- Table3.docx